Journal of Medicinal Chemistry

pubs.acs.org/jmc

Article

# Mechanism of Action of an EPAC1-Selective Competitive Partial Agonist

Hongzhao Shao, Hebatallah Mohamed, Stephen Boulton, Jinfeng Huang, Pingyuan Wang, Haiying Chen, Jia Zhou, Urszula Luchowska-Stańska, Nicholas G. Jentsch, Alison L. Armstrong, Jakob Magolan, Stephen Yarwood, and Giuseppe Melacini*

Cite This: https://dx.doi.org/10.1021/acs.jmedchem.9b02151

Read Online

ACCESS | Metrics & More | Article Recommendations | Supporting Information

**ABSTRACT:** The exchange protein activated by cAMP (EPAC) is a promising drug target for a wide disease range, from neurodegeneration and infections to cancer and cardiovascular conditions. A novel partial agonist of the EPAC isoform 1 (EPAC1), I942, was recently discovered, but its mechanism of action remains poorly understood. Here, we utilize NMR spectroscopy to map the I942−EPAC1 interactions at atomic resolution and propose a mechanism for I942 partial agonism. We found that I942 interacts with the phosphate binding cassette (PBC) and base binding region (BBR) of EPAC1, similar to cyclic adenosine monophosphate (cAMP). These results not only reveal the molecular basis for the I942 vs cAMP mimicry and competition, but also suggest that the partial agonism of I942 arises from its ability to stabilize an inhibition-incompetent activation intermediate distinct from both active and inactive EPAC1 states. The mechanism of action of I942 may facilitate drug design for EPAC-related diseases.

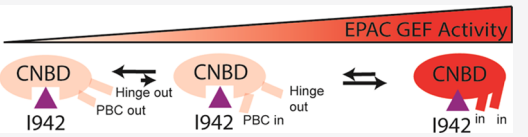




## INTRODUCTION

The exchange proteins activated by cAMPs (EPACs) are a family of guanine nucleotide exchange factors (GEFs) for the GTPases, Rap1, and Rap2.[1,2] EPACs are receptors for the cyclic adenosine monophosphate (cAMP) secondary messenger and contribute to the control of cAMP signaling.[3] EPAC proteins are promising therapeutic targets, as they are involved in multiple physiological effects[4,5] in the nervous,[6,7] cardiovascular,[8−11] endocrine,[12−19] digestive,[20,21] and immune[22−24] systems. Regulation of EPAC activity has been hypothesized to be a viable avenue for developing treatment strategies for Alzheimer's disease,[25] bacterial[22] and viral[23] infections, breast,[18] ovarian,[12,13,17] and pancreatic cancer,[20,21] cardiomyopathy,[8,9] chronic pain,[26,27] diabetes,[14,16] drug dependence,[28] and obesity.[14,16,19]

There are two major isoforms of EPAC, 1 and 2, that share similar structures, but differ in tissue distributions and physiological functions.[3] The EPAC1 isoform is composed of a regulatory region (RR) and a catalytic region (CR). The RR includes the Disheveled Egl-10 Plectstrin (DEP) domain and cyclic nucleotide binding domain (CNBD), while the CR spans the RAS-exchange motif (REM), the RAS association (RA), and CDC25 homology domains (CDC25HD)[4,5,29] (Figure 1A). In its apo form, EPAC1 proteins adopt a primarily closed topology, which autoinhibits GEF activity, as the active site in the catalytic domain is occluded by the RR, which forms multiple salt bridges with the CR, collectively referred to as "ionic latch" (Figure 1A).[30−34]

cAMP modulates EPAC1 allosterically by binding to the CNBD and changing the conformation of the hinge region on the CNBD to its active form. The cAMP binding also allosterically weakens the ionic latch at the N-terminal region of EPAC1-CNBD, causing the release of the catalytic domain from the regulatory domain.[30−34] Upon the release of the catalytic domain from the autoinhibitory RR, it becomes accessible to binding by the Rap1 and Rap2 GTPase substrates, resulting in guanosine diphosphate (GDP) to guanosine triphosphate (GTP) exchange[1,2] (Figure 1A). Hence, the CNBD of EPAC1 serves as its central controlling unit.

The CNBD consists of $\alpha$ and $\beta$ subdomains. The $\alpha$-subdomain starts with an N-terminal $\alpha$-helical bundle (NTHB) that includes helices $\alpha$1−$\alpha$4 as well as the ionic latch residues.[30−35] The $\alpha$-subdomain also comprises helices $\alpha$5 and $\alpha$6, which are distinct from the NTHB, with $\alpha$5 embedded within the $\beta$-barrel and $\alpha$6 located C-terminally to the $\beta$-barrel.[30,34,35] The $\alpha$5 helix is part of the phosphate binding cassette (PBC). The PBC, along with the base binding region (BBR) in the $\beta$-subdomain, is crucial for cAMP docking within the CNBD.[30,34,35] The $\alpha$6 helix is responsible for the hinge rotation of the RR relative to the CR and ultimately for the release of the CR upon binding to cAMP.[30,34,35]

The EPAC1-CNBD undergoes a distinct allosteric conformational change upon binding to cAMP. The simplest model of the

Received: January 2, 2020

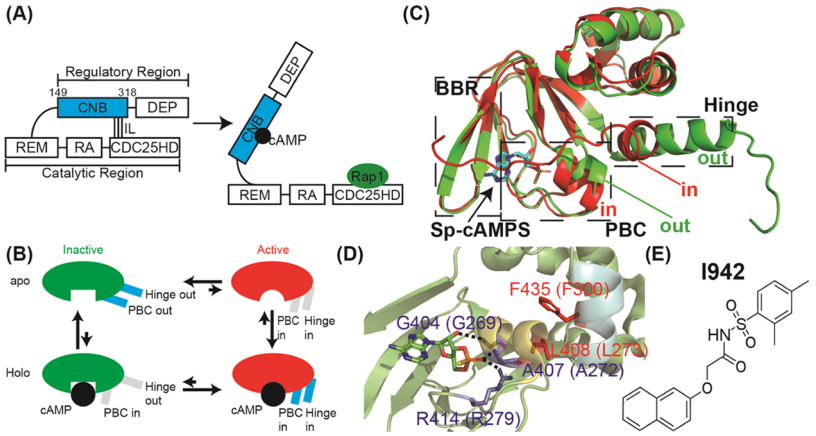


**Figure 1.** Activation mechanism of EPAC1 by cAMP and the covalent structure of the EPAC1 competitive inhibitor I942. (A) Domain organization of EPAC1 and the scheme of EPAC1 activation. The full-length EPAC1 is organized in two major regions, the regulatory and catalytic regions, starting from the regulatory Disheveled Egl-10 Plectstrin (DEP) domain and cyclic nucleotide binding domain (CNBD) and continuing to the catalytic RAS-exchange motif (REM), RAS association (RA), and CDC25 homology domains (CDC25HD). The construct involved in this study is colored blue, with the starting (149) and ending (318) residue numbers stated above. EPAC1 is initially in its autoinhibition state, where an ionic latch (IL) forms between the regulatory and catalytic regions, effectively autoinhibiting EPAC. Upon binding to cAMP in the cyclic nucleotide binding domain, EPAC1 is released from the autoinhibitory state and Rap1 can access the CDC25 homology domain. (B) Thermodynamic cycle coupling the cAMP binding and the EPAC1-CNBD active/inactive equilibria. The EPAC1-CNBD is illustrated in the inactive (green) and active (red) states, where the hinge region and the phosphate binding cassette (PBC) are both in their "out" or "in" conformation, respectively (blue rectangles). The hinge and PBC orientations in the holo-inactive and apo-active states are shown in gray to emphasize that they are only hypothetical. (C) Illustration of the EPAC2-CNBD apo/holo structural differences. The dashed boxes indicate the base binding region (BBR), the phosphate binding cassette (PBC), and the hinge region. The PBC and hinge regions show the out/in conformation shifts from the apo/inactive (green, PDB 2BYV[30]) to the holo/active (red, PDB 3CF6[34]) states. The holo/active state is bound to a known EPAC2 activator, Sp-cAMPS.[34] (D) Structure highlighting Sp-cAMPS bound to EPAC2-CNBD.[34] Hydrogen bonds between Sp-cAMPS and EPAC2 are marked with dashed lines. The interaction between L408 (L273 in EPAC1) in the $\alpha$5 helix (yellow, PBC) and F435 (F300 in EPAC1) in the $\alpha$6 helix (cyan, hinge) is highlighted with red side chains. (E) Covalent structure of the EPAC1 partial agonist I942.

cAMP-dependent allostery in EPAC1 is a four-state thermodynamic cycle arising from the coupling of cAMP binding and conformational equilibria of the CNBD[36−42] (Figure 1B). In the absence of cAMP, the EPAC1-CNBD samples primarily the apo-inactive state, but as the cAMP levels increase the holo-active state is progressively stabilized (Figure 1B). Upon docking in the PBC and BBR, cAMP allosterically affects the conformation of the $\beta$2−$\beta$3 loop and $\alpha$6 hinge helix.[31,33,43] The interaction between cAMP and the PBC is a key driver of the allosteric transition. The cAMP interacts with the PBC primarily through hydrogen bonding and a salt bridge[34,35] (Figure 1D) and changes the conformation of the $\alpha$5 helix in the PBC from an "out" to an "in" orientation, subsequently shifting the orientation of the $\alpha$6 helix (i.e., the hinge region) from "out" to "in"[30,34,35] (Figure 1B,C). The coupling between the PBC and hinge regions relies on the L273−F300 interaction (Figure 1D) and leads to partial unfolding of the $\alpha$6 C-terminal region, closure of the lid, rotation of the regulatory region away from the catalytic region, and ultimately activation of EPAC1.[30,31,34,35]

Given the potential of EPAC as a therapeutic target, over the years, several EPAC selective small-molecule inhibitors were identified through high-throughput screening (HTS).[20,44−53] Recently, a new EPAC1-selective sulfonyl acetamide partial agonist, called I942 (Figure 1E), was discovered through competitive fluorescence. I942 is a promising lead to develop EPAC1-specific partial agonists.[54] Other EPAC agonists have been discovered, but these are cAMP analogs.[55−60] Although some of the cAMP analogs are resistant to phosphodiesterase (PDE) hydrolysis,[59,60] being cyclic nucleotides generally makes most of the cAMP analogs vulnerable to PDE hydrolysis, as cAMP signaling through EPAC1 is subject to PDE4D3 termination.[61,62] Unlike cyclic nucleotides, I942 is less likely to be hydrolyzed by PDEs. Furthermore, cyclic AMP analogues typically exhibit limited membrane permeability and may generate off-target effects. In addition, I942 is significantly more soluble than ESI-09 and CE3F4R, which minimizes nonspecific interactions between I942 and EPAC1.

Using EPAC1 GEF assays, I942 was proven to be able to induce about 10−20% activity compared to cAMP-bound EPAC1.[54] I942 also inhibits the EPAC1 activity induced by cAMP and is therefore classified as a partial agonist.[54] Furthermore, I942 affects multiple EPAC1-dependent cellular functions, including the induction of the suppressor of cytokine signaling 3 (SOCS-3), which in turn suppresses the activation of interleukin 6 (IL-6) signaling, as well as the downstream induction of vascular cell adhesion molecule 1 (VCAM-1) and monocyte adhesion to human umbilical vascular endothelial cells (HUVEC).[63] This could be utilized for the suppression of inflammatory effects and provides an alternative therapeutic approach for the treatment of cardiovascular diseases, including pulmonary artery hypertension and atherosclerosis.[63,64]

To build upon and further improve the I942 lead compound, it is essential to determine its mechanism of action. Unfortunately, only sparse structural information about the complex of EPAC with I942 or cAMP competitive inhibitors is currently available.[64] Hence, here we map, at atomic resolution, the interactions between I942 and the EPAC1-CNBD using NMR spectroscopy. To this end, we have utilized various protein NMR techniques, including chemical shift mapping, saturation transfer difference (STD), nuclear overhauser effect spectroscopy (NOESY), and measurement of intermolecular Nuclear Overhauser Effects (NOEs) through isotope-filtered $^{15}$N-NOESY-HSQC, as well as non-NMR techniques, such as


https://dx.doi.org/10.1021/acs.jmedchem.9b02151
J. Med. Chem. XXXX, XXX, XXX−XXX

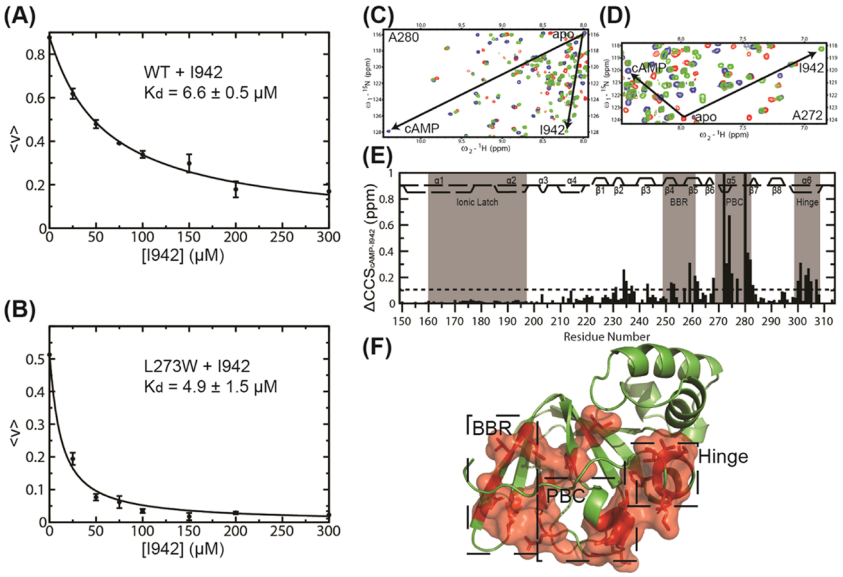


**Figure 2.** I942-binding isotherms for the EPAC1-CNBD and I942 conformations either free or bound to the EPAC1-CNBD and heteronuclear single quantum coherence (HSQC) spectra comparison of the cAMP- and I942-bound EPAC1-CNB domain. (A) Binding isotherm of wild-type EPAC1-CNBD and I942 through 8-NBD-cAMP competition monitored by fluorescence losses. (B) Similar to (A) but for the L273W mutant of the EPAC1-CNBD, which stabilizes the hinge helix in the inactive conformation. In both panels (A) and (B), ⟨v⟩ represents the bound percentage of 8-NBD-cAMP. 2.5 $\mu$M of EPAC1-CNBD and 0.5 $\mu$M of 8-NBD-cAMP were utilized. (C, D) Zoomed-in regions of HSQC spectra of the apo, cAMP-, and I942-bound EPAC1-CNB domain, shown in red, blue, and green, respectively. These regions highlight representative residues from the phosphate binding cassette (PBC). The amides of A280 and A272 donate hydrogen bonds to the cAMP phosphate in the cAMP:EPAC complex.[34] (E) Compounded chemical shift (CCS) differences between the cAMP- and I942-bound EPAC1-CNB domain. Note that any CCS differences over 1 ppm is off-scale. The secondary structure of EPAC1 is marked on the plot along with residue numbers. The dashed line indicates the average ppm value over all residues. (F) 3D map of chemical shifts greater than the average (red surface).

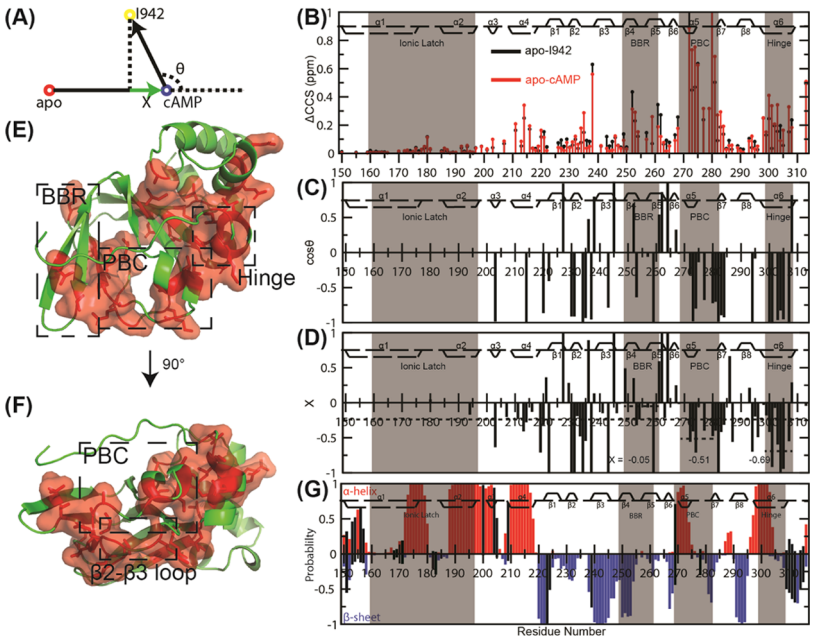


**Figure 3.** CHEemical Shift Projection Analysis (CHESPA) of I942 binding to the EPAC1-CNBD. (A) Vectors included in the CHESPA analysis. (B) Compounded chemical shift (CCS) difference upon binding of cAMP (red) or I942 (black) to the EPAC1-CNBD. (C) cos $\theta$ to measure the extent of linearity of chemical shift changes. (D) Fractional activation ($X$) of I942 relative to cAMP, with dashed lines indicating overall or local averages of the PBC and hinge regions. Values greater than 1 or lower than −1 are off-scale. The secondary structure is plotted along with the residue number in panels (B–D). (E) Map of residues with $X$ values lower than average. (F) Similar to (E), but in a different orientation to display the $\beta$2−$\beta$3 loop. (G) Protein energetic conformational analysis from NMR (PECAN) chemical shift prediction of the secondary structure in the I942-bound EPAC1-CNBD. The secondary structure of apo EPAC1 is plotted along with the residue number. Red bars indicate the probability of residues forming an $\alpha$-helix, while blue bars indicate the probability of residues forming a $\beta$-sheet. Residues without any assignment are marked with black bars and secondary structure probabilities in these regions may be affected by missing data.


https://dx.doi.org/10.1021/acs.jmedchem.9b02151
J. Med. Chem. XXXX, XXX, XXX−XXX

fluorescence. Based on these data, we propose a mechanism of action for the partial agonism exhibited by I942 toward EPAC1.

## RESULTS

**I942 Binds the Inactive and Active States of EPAC1 with Comparable Affinities.** As a first step toward understanding how I942 interacts with EPAC1, we measured the affinity of I942 for the EPAC1-CNBD, i.e., human EPAC1 (149−318), under the same experimental conditions utilized for NMR. For this purpose, the 8-NBD-cAMP analog is a convenient tool[65] since its displacement by I942 causes a loss of 8-NBD-cAMP fluorescence intensity. Hence, monitoring the fluorescence decrease during a I942 titration provides an effective means to measure the affinity of I942 for the EPAC1-CNBD. The effective $K_d$ between I942 and EPAC1-CNBD under our experimental conditions is 6.6 ± 0.5 $\mu$M (Figure 2A), which is comparable to the previously published $K_d$ between cAMP and EPAC1-CNBD of 4.5 ± 0.1 $\mu$M,[66] indicating that I942 is an effective competitive inhibitor of the cAMP-bound EPAC1-CNBD. Furthermore, the $K_d$ value observed for I942 and our EPAC1-CNBD construct does not exceed the $IC_{50}$ and $AC_{50}$ values reported for I942 in the context of a longer EPAC1 construct (i.e., EPAC1 149−881),[54] suggesting that our NMR-amenable construct adequately recapitulates the main determinants of I942 binding to longer EPAC1 constructs.

We also measured the affinity of I942 for the L273W EPAC1 mutant, which is known to prevent activation even in the presence of cAMP.[35] The L273W mutation perturbs the communication between L273 and F300, which is critical for controlling the hinge conformational shift upon cAMP binding. The bulky side chain on the L273W mutant effectively prevents the hinge region from adopting the "in" (or active) conformation even when cAMP binds to the PBC.[35,43] By relying again on 8-NBD-cAMP competitive fluorescence binding experiments, we found that I942 binds to EPAC1-CNBD with a $K_d$ value of 4.9 ± 1.5 $\mu$M (Figure 2B). This result indicates that the silencing of the allosteric network between the PBC and hinge regions through the L273W mutation affects the I942 affinity to the EPAC1-CNBD only marginally. Hence, I942 does not preserve the active vs inactive selectivity of cAMP, which is known to bind the wild-type (WT) EPAC1-CNBD with five-fold higher affinity relative to L273W.[35] These I942 vs cAMP differences provide an initial explanation as to why I942 cannot activate EPAC to an extent similar to cAMP.

**Binding of I942 to the EPAC1-CNBD Maintains Critical Allosteric Sites in the Inactive State.** The $^1H,^{15}N$-HSQC spectrum of the I942-bound EPAC1-CNBD was assigned through comparison with the apo and cAMP-bound spectra as well as through triple-resonance spectra. The overlay of the apo, cAMP- and I942-bound EPAC1-CNBD HSQCs (Figure 2C,D) reveals that I942 causes major perturbations relative to both apo and cAMP-bound states. Marked I942 vs apo chemical shift changes (Figure 3B) are detected for the cAMP-binding sites, i.e., the phosphate binding cassette (PBC) and the base binding region (BBR), in agreement with the cAMP competitive nature of the I942 ligand. Interestingly, significant I942 vs apo chemical shift variations are also observed beyond the PBC and BBR, i.e., at allosteric sites, such as the hinge region and the $\beta2-\beta3$ loop (Figure 3B).

To gain further insight into the nature of the I942-induced perturbations, we also examined the I942 vs cAMP chemical shifts (Figure 2E,F), which reveal major differences at both the cAMP-binding and allosteric sites.[31,67] For example, while hydrogen bonding to the cAMP phosphate causes a major down-field $^1H$ shift for the amides of A280 and A272 in the PBC, as expected based on the H-bonds donated by these backbone amides to the cAMP phosphate, I942 causes only a marginal down-field $^1H$ shift (A280; Figure 2C) or an up-field $^1H$ shift (A272; Figure 2D), pointing to a significant weakening of the intermolecular hydrogen bonds donated by the corresponding amides. Considering that the hydrogen bond with A272 is unique to the active conformation of the EPAC1-CNBD,[35] these differences are fully consistent with the partial agonism previously reported for I942. Overall, the comparative chemical shift analyses of Figure 2C−F reveal that, while I942 targets the PBC and BBR similar to cAMP, the nature of the short-range interactions with the EPAC1-CNBD is markedly different from that of the endogenous effector cAMP. Furthermore, the I942 vs cAMP chemical shift differences at the allosteric sites (Figure 2E,F) point to variations in long-range effects as well.

To further examine the conformational changes induced by I942 binding to the EPAC1-CNBD, CHEmical Shift Projection Analysis (CHESPA) was performed according to the vector definition illustrated in Figure 3A. We found that consistently negative cos $\theta$ and fractional activation values were observed at the PBC and hinge regions (Figure 3C,D), which suggests that I942 induces an inhibitory shift relative to cAMP at these allosteric sites. The shift of the PBC to the inactive state upon replacing cAMP with I942 is also supported by the overall negative CHESPA fractional activation values measured for the $\beta2-\beta3$ loop region, which is adjacent to the PBC (Figure 3F). Although not interacting directly with cAMP, the $\beta2-\beta3$ loop is sensitive to the change in PBC conformation occurring when the EPAC1-CNBD binds to cAMP.[31] Furthermore, the hinge region, which is not a direct cAMP-binding site but is allosterically coupled to the PBC through the L273−F300 side-chain interaction,[31,34,35] is also partially inhibited. The inhibited hinge and PBC regions indicate that, upon displacement of cAMP by I942, the EPAC1-CNBD partially shifts back to the autoinhibited state. Comparing the average of partial inhibition of the PBC and hinge regions, it is clear that I942 inhibits the hinge region more than the PBC (∼50% for PBC vs ∼70% for hinge; Figure 3D). Other sites within the EPAC1-CNBD are subject to similar inhibitory shifts upon replacing cAMP with I942 (Figure 3E,F).

To gain further insight into how I942 affects the structure of EPAC1, we assessed the secondary structure of the I942:EPAC1-CNBD complex using the Protein Energetic Conformational Analysis from NMR chemical shifts (PECAN).[68] The chemical shifts of $^1H$ and $^{15}N$ as well as $^{13}C\alpha$ and $^{13}C\beta$ from $^1N,^{15}H$-HSQC, HNCACB, and HN(CO)-CACB experiments were utilized in the prediction. The prediction results (Figure 3G) indicated that the majority of the secondary structures of cAMP-bound EPAC1-CNBD are preserved upon replacement of cAMP with I942. Outliers include the N-terminal $\alpha1$ and the C-terminal region after $\alpha6$, where most of the assignments are missing due to flexibility and lack of sufficient resolution. In addition, the $\alpha6$ helix in the hinge region was partially unfolded based on this prediction similar to the cAMP-bound EPAC.[34] Another important aspect of the prediction is that the $\alpha5$ helicity in the PBC is retained by I942 binding.

**Conformational Change of I942 upon EPAC1 Binding.** The conformational change of the ligand in the protein−ligand binding process is as important as the conformational shift of the protein receptor. To probe the conformational shift of I942


https://dx.doi.org/10.1021/acs.jmedchem.9b02151
J. Med. Chem. XXXX, XXX, XXX−XXX

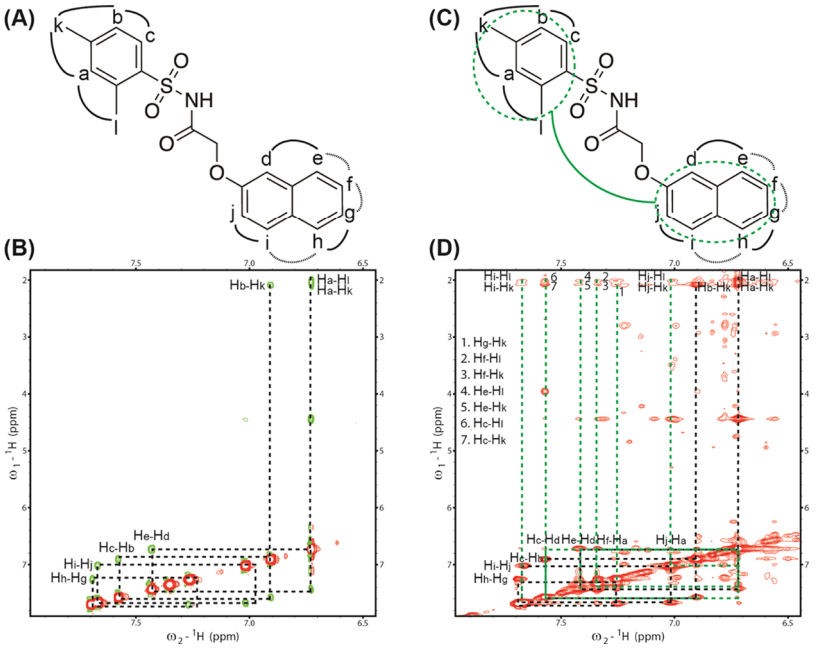


**Figure 4.** Intra-ligand NOEs for the free and the EPAC1-CNB domain-bound I942. The NOESY spectra acquired in the absence and presence of the EPAC1-CNBD construct are shown in panels (B) and (D), respectively. Panels (A) and (C) as well as the dashed lines in spectra (B) and (D) indicate NOE cross-peaks between proton pairs of I942. The black dotted connections in panels (A) and (C) indicate that the chemical shifts of the corresponding protons are too close to result in resolvable cross-peaks. The green lines in C indicate NOEs between the two aromatic moieties. In the presence of EPAC1 the transfer NOE effect prevails, generating cross-peaks of the same sign as the diagonal, whereas in the absence of EPAC1 opposite signs are observed due to the fast tumbling of free I942.

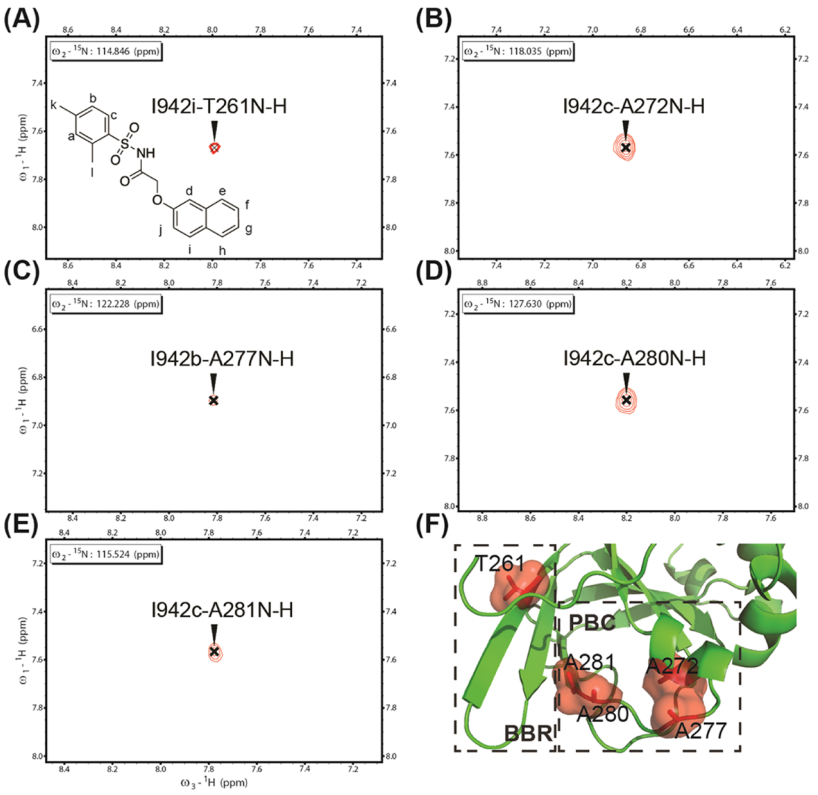


**Figure 5.** Mapping the EPAC1-CNBD and I942 interface. (A–E) Intermolecular NOE peaks from the $^{13}C$, $^{15}N$-filtered NOESY-HSQC spectrum. (F) 3D map of residues identified in the NOESY-HSQC spectrum. Red surfaces indicate the presence of an NOE to I942 originating from the labeled residue.

upon its binding to EPAC1-CNBD, NOESY spectra were acquired for I942 in the absence and presence of the EPAC1-CNBD. In the NOESY spectrum recorded for free I942, several NOEs were observed within each of the aromatic rings, but no


https://dx.doi.org/10.1021/acs.jmedchem.9b02151
J. Med. Chem. XXXX, XXX, XXX−XXX

appreciable NOE was detected between them (Figure 4A,B), pointing to an "open" conformation for I942 before binding to EPAC1. However, in the NOESY spectrum acquired in the presence of substoichiometric amounts of EPAC1-CNBD, several transfer NOEs were observed between the phenyl and naphthalene moieties of I942 (Figures 4C,D and S1), suggesting a less open conformation for I942 bound to the EPAC1-CNBD.

**Intermolecular NOEs, STD-HSQC Data, and I942 Analogs Reveal the Molecular Basis of the I942 vs cAMP Mimicry.** The measurement of intermolecular NOEs between I942 and EPAC1-CNBD is pivotal in mapping the EPAC1:I942 interface. The intermolecular NOEs were acquired with a modified $^{15}$N-NOESY-HSQC pulse program, including two $^{13}$C isotope filters with adiabatic pulses and a $^{15}$N isotope filter. The $^{13}$C, $^{15}$N-filtered, and $^{15}$N-edited experiment distinguishes protons bound to $^{13}$C/$^{15}$N vs $^{12}$C/$^{14}$N atoms and filters out protein−protein intramolecular NOEs within a $^{15}$N/$^{13}$C isotopically labeled protein.[69,70] The experiment resulted in several NOE peaks originating from the backbone of selected PBC and BBR residues (Figure 5A−E). These intermolecular NOEs indicate that the naphthalene and phenyl rings of I942 interact with two different binding regions on EPAC1-CNBD, i.e., the PBC and BBR, respectively (Figure 5F). More specifically, the 2′,4′-dimethylphenyl moiety mimics the ribose ring of cAMP and docks within the PBC, while the naphthalene ring mimics the adenine base of cAMP and docks at the BBR. These results are consistent with STD-HSQC data for the I942:EPAC1-CNBD complex (Figure S2, Supporting Information).

The conclusions drawn based on the intermolecular NOEs were independently verified by comparing the HSQC spectra of the I942- and I942 analog-bound EPAC1-CNBD. We modified the two aromatic moieties and monitored the resulting chemical shift changes in the EPAC1-CNBD.[71] By comparing the chemical shift differences between I942 and analogs with modifications in the 2′,4′-dimethylphenyl ring, we observed that the PBC region exhibits the largest chemical shift differences (Figure 6A−E). The interaction between the naphthalene ring of I942 and the BBR region was probed through a comparison of I942 with an analog of I942 consisting of a naphthalene substitution (Figure 6F). The chemical shift difference analysis showed that in this case it is the BBR region that displays the largest chemical shift differences (Figure 6F). Thus, we confirm that the 2′,4′-dimethylphenyl and naphthalene rings are, in fact, interacting with the PBC and BBR, respectively, in agreement with our intermolecular NOE data.

The engagement of both the 2′,4′-dimethylphenyl and the naphthalene moieties of I942 in contacts with the EPAC1-CNBD was independently confirmed through saturation transfer difference (STD) NMR. STD NMR identifies which groups within I942 are in close contact with the EPAC1-CNBD receptor. STD measures the saturation transfer from protein to ligand, and the STD vs saturation transfer reference (STR) intensity ratio of each proton on I942 reflects the proximity of such protons to the surface of EPAC1[72] (Figure 7A). Figure 7A indicates that the majority of protons exhibit similar STD/STR intensity ratios, confirming their proximity to the EPAC1-CNBD.

While the intermolecular NOEs together with the I942 analogs and the STD data are extremely useful to position I942 within the EPAC1-CNBD, they provide only a limited number of constraints for the sulfonyl group, which is devoid of NMR detectable protons. To further probe to what extent the sulfonyl

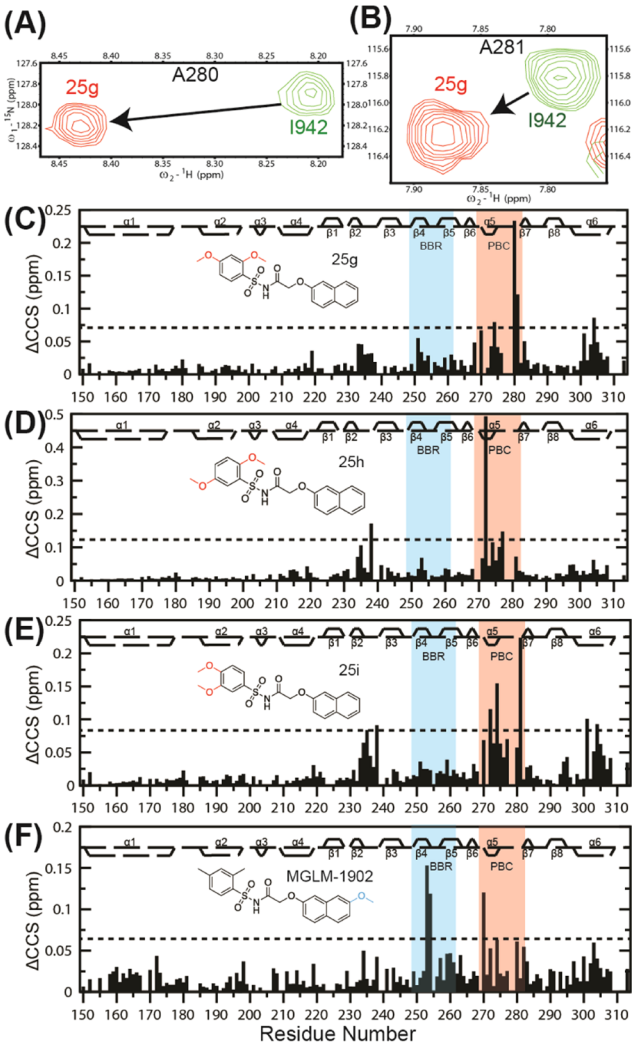


**Figure 6.** Compounded chemical shift differences between I942- and I942 analog-bound EPAC1-CNBDs. (A, B) Representative superimposition of HSQC spectra of EPAC1-CNBD bound to I942 or the I942 analog from panel (C) for residues A280 (A) and A281 (B). (C−F) Compounded chemical shift differences between I942 and I942 analog-bound EPAC1-CNBDs. All CCS differences are plotted along with the residue numbers and the secondary structure. The dashed lines in all plots represent the average plus two standard deviations. The structures of analogs are provided within the plots, with the modifications of I942 colored red or blue to highlight whether they perturb the binding with PBC (red) or BBR (blue).

moiety mimics the cyclic phosphate of cAMP, we complemented the intermolecular NOE measurements with mutations of the PBC arginine residue known to form salt bridges with the cAMP phosphate, i.e., R279.[34]

**Sulfonyl Group on I942 Mimics the Cyclic Phosphate of cAMP and Interacts with the R279 Guanidinium in EPAC1.** I942 contains a sulfonyl group in place of the cyclic phosphate group of cAMP. A viable hypothesis is that the sulfonyl group forms hydrogen bonds and/or salt bridges with the R279 side-chain guanidinium group[34] similar to cAMP. To test this hypothesis, we acquired guanidinium HSQC spectra and selectively assigned the R279 guanidinium group through the R279A mutant. If cAMP stabilizes the guanidinium of R279 by forming hydrogen bonds or salt bridges and by reducing the rate of rotation of its $NH_2$ moieties to fall within the slow exchange limit, all N−H signals arising from the guanidinium's


https://dx.doi.org/10.1021/acs.jmedchem.9b02151
J. Med. Chem. XXXX, XXX, XXX−XXX

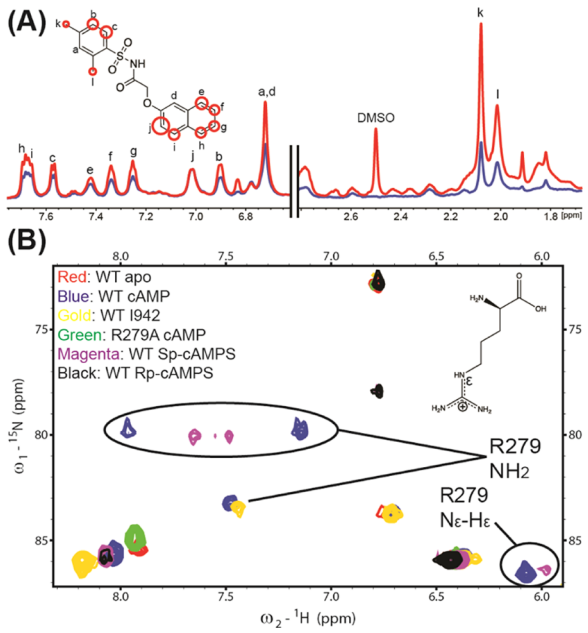


**Figure 7.** Interactions between I942 and EPAC1-CNBD mapped by saturation transfer difference and guanidinium HSQC. (A) Saturation transfer difference and group epitope mapping for I942 binding to the EPAC1-CNB domain. The 1D STR (red) and STD (blue) spectra are overlayed. The STD spectrum is rescaled so that the intensities of proton *j* in both spectra match. Proton j was selected as it exhibits the maximum STD/STR ratio. The assignments of the spectra are indicated through the labels in the molecular structure, whereas the radii of the red circles indicate the relative normalized STD/STR ratios. (B) Guanidinium HSQC spectra. The spectra overlay includes the R279A mutant and the WT of the EPAC1-CNB domain in the apo form or saturated with different ligands, as per the legend in the spectra. The circled peaks are assigned to the -$NH_2$ and $N_\varepsilon$–$H_\varepsilon$ guanidinium moieties of Arginine 279.

two $NH_2$ groups and $N_\varepsilon$–$H_\varepsilon$ bond are expected to be visible in the HSQC spectrum of the cAMP-bound WT EPAC1-CNBD domain. These signals should be also expected to disappear and/or move upon removal of either cAMP (i.e., in the WT apo sample) or the R279 guanidinium (i.e., in the R279A cAMP-bound sample). Figure 7B shows the peaks in the Arg-HSQC spectrum of cAMP-bound EPAC1-CNBD that meet these criteria and were therefore assigned to the guanidinium of R279.

Interestingly, the Arg-HSQC spectrum of I942-bound WT EPAC1-CNBD preserves the signals from only one of the two $NH_2$ groups of R279 observed for the cAMP-bound WT EPAC1-CNBD. To gauge the allosteric role of the two R279 $NH_2$ groups, we then acquired Arg-HSQC spectra for Sp-cAMPS-bound WT EPAC1-CNBD. Sp-cAMPS is a well-known superagonist of EPAC in which the axial exocyclic oxygen of the cyclic phosphate group is replaced by a sulfur atom. Sulfur is bulkier and more polarizable than oxygen and therefore perturbs hydrogen bonds and salt bridges involving the cyclic phosphate. Comparative analysis of the Arg-HSQC spectra of the Sp-cAMPS- and I942-bound samples shows that Sp-cAMPS and I942 preserve clearly different arginine $NH_2$ signals, indicating that, unlike Sp-cAMPS, I942 is unable to engage the R279 $NH_2$ group necessary for activation, while still forming hydrogen bonds and/or salt bridges with the other R279 $NH_2$ moiety. These observations provide a further rationale to explain the molecular basis of the I942 partial rather than full agonism. On the other hand, the R279 guanidinium spectrum of I942 differs from the corresponding spectrum measured in the presence of the reverse-agonist Rp-cAMPS (Figure 7B), consistent with the ability of I942 to partially activate EPAC1. To further probe how I942 affects the allosteric network of EPAC1, we relied on the CHEmical Shift Covariance Analysis (CHESCA).

**CHESCA Reveals How I942 Perturbs the Allosteric Network of the EPAC1-CNBD.** The allosteric network within the EPAC1-CNBD is critical to release EPAC1 from autoinhibition. Previously, the allosteric network of the EPAC1-CNBD was identified through an NMR chemical shift analysis method called CHEmical Shift Covariance Analysis (CHESCA).[67] The previously determined correlation matrix reveals a strong correlation of the hinge region with both the PBC and the $\alpha$4 helix.[67] The allosteric network between the hinge region and the PBC is critical for EPAC1 activation. The residue pair L273–F300 between the PBC and the hinge region controls the position of the autoinhibitory equilibrium of EPAC1,[34] whereas the allosteric network between the hinge region and the adjacent $\alpha$4 helix is sensitive to the orientation of the hinge region, as the $\alpha$4 helix preserves a similar conformation in the active and inactive form.[30,34,35]

To examine how I942 perturbs the EPAC1-CNBD allosteric network, the cAMP CHESCA perturbation was replaced with I942 and the CHESCA computed (Figure 8B). A control CHESCA with cAMP-bound EPAC1-CNB including an I942-matching amount of dimethyl sulfoxide (DMSO-$d_6$) was also performed to minimize the potential effects arising from the addition of DMSO-$d_6$ (Figure 8A). Upon replacing cAMP with I942, we observed a significant loss of correlations relative to the control CHESCA (Figure 8). Despite such loss, the I942 matrix still retained multiple correlations of the hinge region with the $\alpha$4 helix as well as the PBC (Figure 8B). Selected correlations between the hinge and the $\alpha$4 helices were either weakened or lost, i.e., most of the correlations between residues Q298, D299, E308, and the $\alpha$4 helix were retained (Figure S3), whereas most of the correlations between F300, N301, V307, and $\alpha$4 helix were lost (Figure S3). These correlations between the hinge region and its adjacent region, the $\alpha$4 helix, are an indicator of whether the hinge region adopts a third conformation other than the common "in" or "out" orientation.

Another critical aspect of the allosteric network regulating EPAC1 activation is the coupling between the hinge region and the PBC, which controls the orientation of the hinge ($\alpha$6) helix.[30,34,35] The L273–F300 pair-wise correlation exhibits an absolute Pearson correlation coefficient of 0.97 in the control CHESCA (Figure 8C) and 0.98 in the I942-CHESCA (Figure 8D), with I942 partitioned between the inactive apo state and the agonist states, i.e., I942 falls in the partial activator category (Figure 8D). A residue close to L273, i.e., N275, is another interesting case. Its correlations with F300, I303, and V307 (Figure S4A, S4B) were lost with the I942-CHESCA, while its correlation with E308 was retained and I942 acts as an activator (Figure S4C,D). Overall, while some key pair-wise residue correlations remain after I942 binding, e.g., L273–F300, several other correlations between the two helices are lost, suggesting that in the presence of I942, the $\alpha$6 helix samples a conformational ensemble that is distinct from the traditional structures of apo- and cAMP-bound EPAC1 involved in the two-state model previously proposed to explain EPAC1 activation. In the simplest case, these observations point to a three-state partial agonism model for I942.


https://dx.doi.org/10.1021/acs.jmedchem.9b02151
J. Med. Chem. XXXX, XXX, XXX–XXX

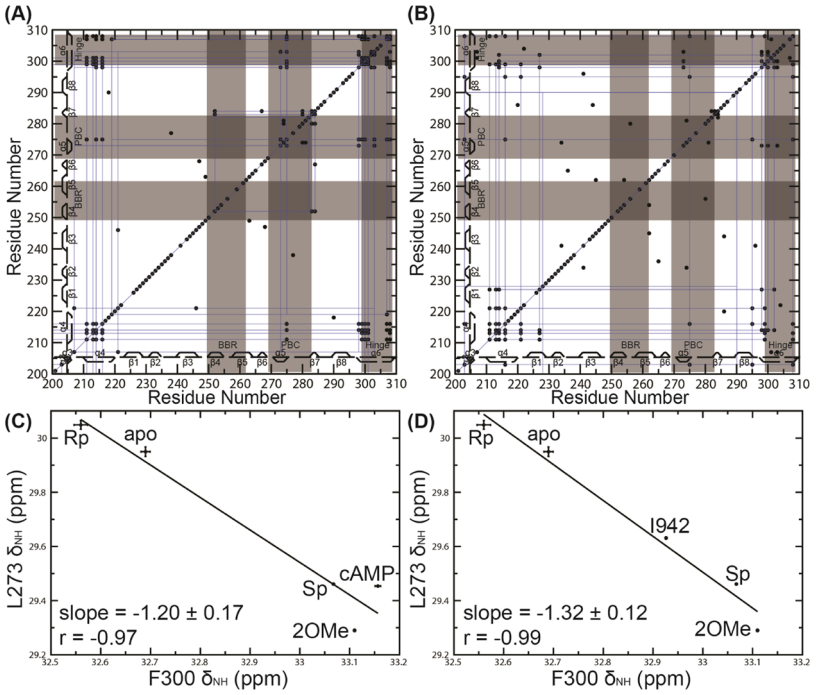


**Figure 8.** CHESCA and the allosteric networks perturbed by I942 binding. (A, B) CHEmical shift correlation matrices from CHESCA. All secondary structures are plotted along with the residue number. Each point represents a residue pair with a Pearson correlation coefficient ≥ 0.98 and residues identified to belong to the major cluster from agglomerative clustering are connected with blue lines. Each matrix includes the apo and the 2′-OMe-cAMP, Rp-cAMPS, Sp-cAMPS-bound EPAC1-CNBDs, and the DMSO-$d_6$ matched cAMP- (A) or I942- (B) bound EPAC1-CNBDs. (C, D) Pairwise residue vs residue chemical shift correlation between L273 and F300 with cAMP (C) or I942 (D).

## DISCUSSION AND CONCLUSIONS

Based on the available data, here we propose a viable mechanism of action for I942 as a partial agonist for EPAC1 (Figure 9). First, our NMR analyses reveal the molecular basis of the I942 vs cAMP mimicry. The 2,4-dimethylphenyl group, the sulfonyl group, and the naphthalene ring of I942 mimic the ribose ring, the cyclic phosphate, and the adenine base of cAMP, respectively (Figure 9A). This conclusion is independently confirmed by our intermolecular NOE and chemical shift data. In particular, multiple intermolecular NOEs were detected between the PBC and the 2′,4′-dimethylphenyl moiety as well as between the BBR and the naphthalene ring, confirming that the 2′,4′-dimethylphenyl ring and the naphthalene moieties bind to the cAMP ribose and base docking regions, respectively, in full agreement with the I942 analog chemical shift data (Figure 6). In addition, considering that, when bound to EPAC1, cAMP adopts a *syn* conformation with the adenine base pointing toward the ribose,[73] the phenyl-ribose/naphthalene-adenine I942 vs cAMP mimicry proposed here suggests proximity between the phenyl and naphthalene rings for EPAC1-bound I942. This prediction is fully consistent with the transition to a less open conformation observed for I942 upon EPAC1 binding.

The replacement of cAMP in the EPAC1-CNBD by I942 results in three main effects on EPAC1:

(a) It compromises selected intermolecular hydrogen bonds with the PBC, which are necessary to fully engage the PBC in an active conformation (Figure 9B). For example, comparative chemical shift analyses clearly indicate that the hydrogen bonds with the amides of A272 and A280 in the PBC are significantly weaker in the I942:EPAC1 vs cAMP:EPAC1 complex (Figures 2C,D and 9B) and that I942 significantly perturbs the salt bridge with the allosterically critical guanidinium of R279 (Figures 7B and 9B). The guanidinium HSQC spectra indicate that only one $NH_2$ group of Arginine 279 is involved in the formation of a salt bridge with the sulfonyl group in I942 and that this $NH_2$ group is different from the one engaged by the superagonist Sp-cAMPS (Figure 7B).

(b) The I942 vs cAMP exchange also perturbs the allosteric network between the PBC and the hinge helix, as indicated by comparative CHESCA analyses (Figures 8 and S3 and S4).

(c) The I942 vs cAMP replacement induces a partial inhibitory shift of the PBC and hinge regions from the "in" to the "out" orientation. While the partial in-to-out shift affects both the PBC and hinge regions, the PBC on average favors the "in" orientation more than the hinge region (Figure 3D). The differential in-to-out transition of the PBC vs hinge sites is consistent with the compromised allosteric couplings observed by CHESCA for the I942-bound EPAC1-CNB domain and is explained through the partial stabilization by I942 of a third "mixed" intermediate with a PBC-in and hinge-out topology (Figure 9C). The population of active and inactive populations was estimated through the fractional activation values from CHESPA (Figure 3D). The active population was estimated through the fractional activation values from the hinge region. The hinge region was ∼70% inhibited, so the active population could be estimated at ∼30%. Similarly, the inactive population was estimated through the PBC inhibition at ∼50%. Hence, the inactive population was estimated to be ∼50%. There was ∼20% population that was unaccounted for, which was assigned to the mixed intermediate state.


https://dx.doi.org/10.1021/acs.jmedchem.9b02151
J. Med. Chem. XXXX, XXX, XXX−XXX

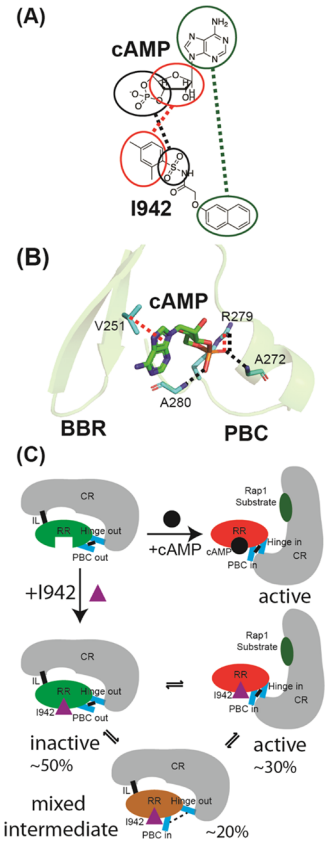


**Figure 9.** Proposed mechanism of action of I942 as a partial agonist for EPAC1. (A) Molecular basis for the I942 vs cAMP mimicry. Circles and dashed lines indicate how I942 mimics cAMP when bound to EPAC1. (B) Illustration of the interactions preserved or perturbed by I942 compared to cAMP. Interactions disrupted by I942 binding are depicted by black dashed lines and interactions largely preserved by I942 binding are shown as red dashed lines. In the case of the R279 guanidinium group, both types of lines are present because of only partial perturbation by I942. (C) Proposed mechanism of action of I942 as a partial agonist for EPAC1. The scheme includes the activation of EPAC1 by cAMP binding for comparison purposes and a three-state equilibrium for the I942:EPAC1-CNBD complex. The mixed intermediate includes elements from both active and inactive states of the EPAC1-CNBD.

The presence of the mixed PBC-in/hinge-out intermediate in the conformational ensemble sampled by the I942:EPAC1-CNBD complex is also supported by the comparable WT vs L273W affinities of I942 (Figure 2A,B). L273W is known to stabilize such mixed intermediates through the interposition of the bulky indole side chain between the PBC and the hinge helices. Hence, the partial agonism of I942 does not arise from a simple shift of the original two-state active vs inactive conformational equilibrium but is in agreement with the presence of a mixed PBC-in/hinge-out intermediate state (~20%).[30,33−35] Considering that the hinge-in orientation is necessary for full activation, such an intermediate is expected to be inhibitory, thus rationalizing the partial agonism observed for I942 in GEF assays.[54] Overall, the model of Figure 9C suggests that the disengagement of the CNBD hinge helix is the primary factor limiting I942 agonism. The proposed mechanism of I942 partial agonism provides a basis for the design of the next generation of I942 analogs with improved potency and efficacy.

## EXPERIMENTAL SECTION

**Protein Expression and Purification.** The human EPAC1 (149−318) construct, referred here as EPAC1-CNBD, as wild-type, R279A, or L273W mutants, was expressed and purified based on previously described protocols.[31,52,67,73] In summary, a GST (Glutathione S-transferase)-tagged fusion protein clone was transformed into the *E. coli* BL21 (DE3) strain on ampicillin-infused LB (Lysogeny Broth) agar. A well-isolated colony was picked and grown in LB broth for 6 h and then inoculated in $^{15}N$- or $^{15}N/^{13}C$-labeled M9 minimal media depending on the requirement of nuclei for the NMR experiments. The inoculated culture was incubated at 37 °C until the optical density at 600 nm reached the 0.6−0.8 range. The grown culture was then induced with 0.5 mM of isopropyl $\beta$-D-1-thiogalactopyranoside (IPTG) and incubated at 18−20 °C for 16−18 h. Cells were harvested and lysed with either a cell disruptor or a sonicator in a lysis buffer composed of phosphate-buffered saline, 10% glycerol, 10 mM of ethylenediaminetetraacetate (EDTA), 1 mM of dithiothreitol (DTT), 12 $\mu$g of $N_\alpha$-*p*-tosyl-L-lysine-chloromethyl ketone (TLCK) and 12 $\mu$g of *N*-*p*-tosyl-phenylalanyl-chloromethyl ketone (TPCK), and 0.24 mM of 4-(2-aminoethyl)benzenesulfonyl fluoride (AEBSF), pH 7.4. The cell lysate was purified with a Glutathione Sepharose 4B resin (GE Healthcare). First, the resin was washed with 50 mM Tris, 500 mM NaCl, and 1 mM DTT, pH 8.0, and later washed and suspended in 50 mM Tris, 50 mM NaCl, and 1 mM DTT, pH 7.6. The GST-tag was removed by treating with biotinylated thrombin (EMD-Millipore) for 12−16 h, and the biotinylated thrombin was later removed using a Streptavidin Sepharose High Performance resin (GE Healthcare). The crude product was further purified with a HiTrap Q HP anion exchange chromatography column (GE Healthcare) and dialyzed in 50 mM Tris, 50 mM NaCl, and 1 mM DTT, pH 7.6, overnight.

**NMR Sample Preparation and NMR Spectroscopy.** The final dialysis buffer mentioned in the previous paragraph was also utilized as buffer for the NMR experiments and the 8-NBD-cAMP competitive binding titration, except when a buffer devoid of detectable protons was required, as specified below. The latter is composed of 20 mM sodium phosphate buffer and 50 mM NaCl in $D_2O$, pH 7.6. The I942 ligand (Life Chemicals; purity >99%), i.e., *N*-((2,4-dimethylphenyl)sulfonyl)-2-(naphthalen-2-yloxy)acetamide, was dissolved in deuterated DMSO-$d_6$ as a stock with 50 mM concentration and diluted with the appropriate experiment-specific buffer, as described below, when needed. All NMR experiments were carried out on a Bruker Avance 700 MHz spectrometer equipped with a 5 mm TCI cryo-probe, unless otherwise specified. Experiments were performed at a temperature of 306 K except for ligand-based experiments, such as saturation transfer difference (STD) and 2D transfer NOESY, which were conducted at 298 K for more efficient cross-relaxation. All samples for NMR spectroscopy prepared with DMSO-$d_6$ had a DMSO-$d_6$ content $\leq$ 2% v/v to minimize potential chemical shift perturbations from the addition of DMSO-$d_6$,[45] and all samples in nondeuterated buffer were supplied with 5% v/v of $D_2O$ for locking purposes. A matching amount of DMSO-$d_6$ was added to apo and cAMP-bound EPAC as a control for DMSO-$d_6$-induced chemical shift changes. The 1D experiments were processed and analyzed with TopSpin (Bruker), and the 2D/3D experiments were processed with Topspin and/or NMRPipe[74] and analyzed with Sparky.[75] The assignment of the I942 1D spectrum was determined based on COSY and TOCSY experiments (Figure S5). The I942-bound EPAC1-CNBD NMR spectra were assigned through comparisons with apo and cAMP-bound spectra as well as 3D triple-resonance experiments. Details of NMR experimental acquisitions are described below.

**Saturation Transfer Difference (STD) and Group Epitope Mapping.** The binding between the EPAC1-CNBD and I942 was probed by STD experiments. A 50 $\mu$M EPAC1-CNB domain sample was buffer-exchanged into 20 mM sodium phosphate buffer supplied with 50 mM of NaCl, pH 7.6, in 99.9% $D_2O$ with Zeba Spin Desalting Columns of 7K MWCO (Thermo Scientific). I942 was added to the EPAC1-CNBD at 300 $\mu$M. The samples were incubated at room temperature for at least 30 min to ensure that protein−ligand binding reached its equilibrium prior to NMR acquisition. Saturation transfer


https://dx.doi.org/10.1021/acs.jmedchem.9b02151
J. Med. Chem. XXXX, XXX, XXX−XXX

reference (STR) experiments were acquired with an off-resonance saturation at 30 ppm, whereas STD experiments were acquired with an on-resonance saturation at 0.85 ppm, where the methyl region of EPAC1 appears and no I942 1D signal is detected. Hence, the STD experiment monitors saturation transfer from EPAC1 to I942. The spectral width was set at 11.9807 ppm with a transmitter frequency of 4.717 ppm for both STD and STR spectra. The STD experiment was performed with 512 scans and the STR experiment with 256 scans, along with 8 dummy scans for both. The STD/STR signal intensity ratios for different I942 peaks were computed and normalized to the largest STD/STR ratio to probe the binding group epitope mapping.[72]

**2D-NOESY.** The conformational changes between free and EPAC1-CNB-bound I942 were probed by NOESY and transfer NOESY experiments. EPAC1-CNBD (50 $\mu$M) was buffer-exchanged into the same buffer as the STD experiments with Zeba Spin Desalting Columns of 7K MWCO (Thermo Scientific) and 300 $\mu$M of I942 was added to the sample. Additional NOESY spectra of 100 $\mu$M of free I942 and 50 $\mu$M of free EPAC1-CNBD were also acquired as the free ligand and free protein controls, respectively. All NOESY spectra were acquired with 2048 and 512 or 256 complex points in the direct and indirect dimensions, respectively, 64 dummy scans, 64 scans, and spectral widths of 11.9807 ppm with a transmitter frequency of 4.696 ppm. The NOESY mixing time was 250 ms in the presence of the EPAC1-CNBD and 750 ms for free I942.

**Measurement of Intermolecular NOEs.** Intermolecular NOEs were measured through isotopically filtered NOESY-HSQC experiments. The intermolecular NOEs between the $^{15}N/^{13}C$-labeled EPAC1-CNBD and I942 were measured with samples in a non-deuterated buffer because the protein HN backbone would otherwise exchange with $D_2O$ and eliminate any NOEs with exchangeable NH amides. $^{15}N$- and $^{13}C$-isotopic filters with $^{13}C$ adiabatic pulses were implemented in the $^{15}N$-NOESY-HSQC pulse sequence to measure intermolecular NOEs.[69,70] The experiment was acquired at 306 K with 128 dummy scans, 8 scans, and complex points of 1024, 256, and 128 in the $^1H$ direct, $^1H$ indirect, and $^{15}N$ dimensions, respectively, and spectral widths of 13.9, 14.0, and 32.0 ppm, respectively. The transmitter frequency was set at 4.7 and 119.0 for the $^1H$ and $^{15}N$ channels, respectively. The $^{15}N/^{13}C$-filtered NOESY-HSQC was acquired with a mixing time of 150 ms. We also recorded a $^{15}N$-edited NOESY-HSQC spectrum on the $^{15}N,^{13}C$-labeled EPAC1 (149−318) with a mixing time of 250 ms and without $J_{13C\text{-}1H}$ refocusing or decoupling pulses to confirm the intermolecular NOEs.

**Guanidinium HSQC.** The side-chain guanidinium group $^{15}N$ signals resonate generally at around ∼85 ppm,[76] which is usually not within the spectral width of routine HSQC experiments and far from the $^{15}N$ carrier frequency, resulting in offset effects. Here, we changed the $^{15}N$ carrier frequency to 80 ppm and expanded the HSQC $^{15}N$ spectral width to monitor the guanidinium groups in arginine side chains. To evaluate the involvement of the EPAC1 Arginine 279 side-chain guanidinium NH and $NH_2$ moieties in I942 binding, guanidinium HSQC spectra were acquired for wild-type apo, cAMP-, and I942-bound states as well as the R279A mutant in the cAMP-bound state to assign the N−H peaks corresponding to the R279 guanidinium. To improve the signal-to-noise ratio, the number of scans was increased to 64. A guanidine HSQC of the Sp-cAMPS-bound wild-type EPAC1-CNBD was also acquired to confirm which $NH_2$ group of R279 is involved in I942 binding, since the crystal structure of Sp-cAMPS-bound EPAC2-CNB is known.[34]

**STD-HSQC.** STD-$^{13}C$-HSQC spectra were recorded to monitor the saturation transfer from I942 to the EPAC1-CNB domain. The STD/STR-$^{13}C$-HSQC spectra were acquired in $D_2O$ to minimize residual water artifacts in the spectrum. Two samples of 250 $\mu$M in the EPAC1-CNB domain with and without 1 mM of I942 were prepared. The apo sample was prepared for saturation transfer leak through control purposes. Both the STR-HSQC and STD-HSQC spectra were acquired at 306 K with 64 dummy scans, 1024 ($^1H$) and 256 ($^{13}C$) complex points, spectral widths of 13.0301 ppm ($^1H$) and 90.0 ppm ($^{13}C$), and transmitter frequencies at 1.0 ppm ($^1H$) and 39.0 ppm ($^{13}C$). The STR-HSQC spectrum was acquired with 8 scans, while the STD-HSQC spectrum was acquired with 64 scans as the STD-HSQC experiment is less sensitive compared to STR-HSQC. In addition, the STD-HSQC experiment was acquired with an irradiation of I942 naphthalene signals to monitor saturation transfer from I942 to EPAC1.

**8-NBD-cAMP Competitive Binding.** I942 competes with 8-(2-[7-nitro-4-benzofurazanyl] aminoethylthio) adenosine-3′,5′-cyclic monophosphate (8-NBD-cAMP) for binding to the EPAC1-CNB domain, and the $K_d$ of the EPAC1-CNBD:I942 complex was determined through the loss of fluorescence intensity of 8-NBD-cAMP bound to EPAC1-CNBD.[65] A series of I942 samples with concentrations ranging from 0 to 300 $\mu$M was added to mixtures of 2.5 $\mu$M of EPAC1-CNB and 0.5 $\mu$M of 8-NBD-cAMP in the NMR buffer. The samples were incubated at room temperature for at least 30 min to promote protein−ligand binding equilibrium and loaded onto Corning 96-well half area plates afterward. The plate was scanned with a Cytation 5 plate reader (BioTek) using an excitation wavelength of 485 nm and an emission wavelength of 535 nm. The competitive binding was fitted as previously described.[77] The bound 8-NBD-cAMP percentage ($\langle v \rangle$) is plotted against the total concentration of I942. The percentage of bound 8-NBD-cAMP can be described as

$$\langle v \rangle_{8-\mathrm{NBD-cAMP}} = \frac{-a + 2\sqrt{a^2 - 3b}\,\cos\left(\frac{\theta}{3}\right)}{3K_{\mathrm{d,8-NBD-cAMP}} - a + 2\sqrt{a^2 - 3b}\,\cos\left(\frac{\theta}{3}\right)}$$

where

$$a = K_{\mathrm{d,8-NBD-cAMP}} + K_{\mathrm{d,I942}} + [8 - \mathrm{NBD{-}cAMP}]_T + [\mathrm{I942}]_T - [\mathrm{EPAC}]_T$$

$$b = K_{\mathrm{d,8-NBD-cAMP}}K_{\mathrm{d,I942}} + K_{\mathrm{d,I942}}([8 - \mathrm{NBD} - \mathrm{cAMP}]_T - [\mathrm{EPAC}]_T) + K_{\mathrm{d,8-NBD-cAMP}}([\mathrm{I942}]_T - [\mathrm{EPAC}]_T)$$

$$c = -K_{\mathrm{d,8-NBD-cAMP}}K_{\mathrm{d,I942}}[\mathrm{EPAC}]_T$$

$$\theta = \arccos\frac{-2a^3 + 9ab - 27c}{2\sqrt{(a^2 - 3b)^3}}$$

The errors on the $K_d$ and $\langle v \rangle$ values were computed as the standard deviations of replicate measurements. The reported $K_d$ values are the average of replica experiments.

**Chemical Shift Analysis.** The chemical shift projection analysis (CHESPA) was performed similarly to what previously described[43,78] with both apo and cAMP-bound EPAC1-CNBD samples supplied with 2% DMSO-$d_6$ to match the DMSO-$d_6$ content in I942-bound EPAC1-CNBD sample. The compounded chemical shift difference (ΔCCS), cos $\theta$, and fractional activation (X) (Figure 3A) were computed as

$$\Delta\mathrm{CCS} = \sqrt{(\Delta\delta H)^2 + (0.2\times\Delta\delta N)^2} \quad (1)$$

$$\cos\theta = \frac{A\cdot B}{|A||B|}$$

$$X = \frac{|A|}{|B|}\cos\theta$$

The cos $\theta$ and fractional activation (X) were computed with a minimum cutoff of 0.05 ppm for the ΔCCS of vectors A (perturbation) or B (reference). The CHEmical Shift Covariance Analysis (CHESCA) was also performed with five different states: apo, cAMP or I942, 2′-OMe-cAMP, Rp-cAMPS, and Sp-cAMPS bound as previously described[67,78] to probe the allosteric perturbations caused by I942. First, the compounded chemical shifts (CCS) were calculated for each residue in every spectrum.

$$\delta_{\mathrm{NH}} = 0.2 \times \delta_{\mathrm{N}} + \delta_{\mathrm{H}}$$

Pair-wise residue linear correlations were then identified by computing the correlation matrix of the transpose of the residue × state CCS matrix. An absolute value Pearson correlation coefficient cutoff of 0.98 was used. The cAMP, 2′-OMe-cAMP, and Sp-cAMPS samples served as references for the active states of the EPAC1-CNBD, while the apo


https://dx.doi.org/10.1021/acs.jmedchem.9b02151
J. Med. Chem. XXXX, XXX, XXX−XXX

and Rp-cAMPS samples as references for the inactive states in the CHESCA analysis. Then, the cAMP-bound state was replaced with the I942-bound state. Except for I942-bound EPAC1-CNBD, all spectra for the CHESCA analysis were acquired previously, unless otherwise specified.[67] After the assembly of the two matrices with cAMP or I942 along with the other CHESCA perturbation states, the allosteric network differences occurring upon replacing cAMP with I942 were identified through the comparative analysis of the two chemical shift correlation matrices. A control CHESCA with cAMP replaced by cAMP in an I942-matching amount of DMSO-$d_6$ was also performed to minimize any effect caused by DMSO-$d_6$. The errors for the I942-bound EPAC1-CNBD-compounded chemical shifts were estimated through a technical triplicate, and the errors of cAMP-bound EPAC1-CNBD with matching DMSO-$d_6$ were calculated through previously published cAMP-bound spectra.[67] The chemical shift correlation matrices served as the input for agglomerative clustering using Cluster 3.0[79] to find EPAC1-CNBD residue clusters that represent functional allosteric networks. The clustering was performed through the complete linkage method, and all clusters were extracted with a correlation coefficient cutoff value of 0.95.

**Validation of the I942:EPAC1-CNBD Interactions through the Chemical Shift Differences Induced by I942 Analogs.** HSQC spectra of several I942 analog-bound EPAC1-CNBD samples were acquired to validate the I942−EPAC1-CNBD interactions. The analogs contained modifications in the 2′,4′-dimethylphenyl[80] and naphthalene moieties. Purity was confirmed by LC−MS to be ≥ 95% for all compounds used. The compounded chemical shift differences between the I942 and its analog-bound states were computed using eq 1 to probe the location of the protein residues perturbed by the ligand modifications.

**Estimation of State Populations in the Three-State Equilibrium.** The populations of the inactive, active, and intermediate states were estimated through the fractional activation values obtained from CHESPA, as previously described.[78,81,82] For instance, the active state is the only state in which the hinge adopts the "in" orientation as opposed to the "out" orientation in the inactive and intermediate states. On the other hand, the inactive state is the only state in which the PBC adopts the "out" orientation as opposed to the "in" orientation in the active and intermediate states. Hence, both active and inactive populations were calculated through the local average fraction activation of the hinge and PBC regions, respectively. The intermediate state accounts for the remaining population percentage other than the active and inactive states.

## ■ ASSOCIATED CONTENT

### Supporting Information

The Supporting Information is available free of charge at https://pubs.acs.org/doi/10.1021/acs.jmedchem.9b02151.

Supporting Figures S1−S5; additional results; synthesis experimental section; compound purity section (PDF)

Molecular formula strings (CSV)

## ■ AUTHOR INFORMATION


### Corresponding Author

**Giuseppe Melacini** − *Department of Chemistry and Chemical Biology and Department of Biochemistry and Biomedical Sciences, McMaster University, Hamilton, Ontario L8S 4L8, Canada;* orcid.org/0000-0003-1164-2853; Email: melacin@mcmaster.ca

### Authors

**Hongzhao Shao** − *Department of Chemistry and Chemical Biology, McMaster University, Hamilton, Ontario L8S 4L8, Canada*

**Hebatallah Mohamed** − *Department of Chemistry and Chemical Biology, McMaster University, Hamilton, Ontario L8S 4L8, Canada*

**Stephen Boulton** − *Department of Biochemistry and Biomedical Sciences, McMaster University, Hamilton, Ontario L8S 4L8, Canada;* orcid.org/0000-0002-2521-2240

**Jinfeng Huang** − *Department of Chemistry and Chemical Biology, McMaster University, Hamilton, Ontario L8S 4L8, Canada*

**Pingyuan Wang** − *Chemical Biology Program, Department of Pharmacology and Toxicology, University of Texas Medical Branch, Galveston, Texas 77555, United States*

**Haiying Chen** − *Chemical Biology Program, Department of Pharmacology and Toxicology, University of Texas Medical Branch, Galveston, Texas 77555, United States*

**Jia Zhou** − *Chemical Biology Program, Department of Pharmacology and Toxicology, University of Texas Medical Branch, Galveston, Texas 77555, United States;* orcid.org/0000-0002-2811-1090

**Urszula Luchowska-Stańska** − *Institute of Biological Chemistry, Biophysics and Bioengineering, School of Engineering and Physical Sciences, Heriot-Watt University, Edinburgh EH14 4AS, United Kingdom*

**Nicholas G. Jentsch** − *Department of Biochemistry and Biomedical Sciences, McMaster University, Hamilton, Ontario L8S 4L8, Canada*

**Alison L. Armstrong** − *Department of Chemistry and Chemical Biology and Department of Biochemistry and Biomedical Sciences, McMaster University, Hamilton, Ontario L8S 4L8, Canada*

**Jakob Magolan** − *Department of Biochemistry and Biomedical Sciences, McMaster University, Hamilton, Ontario L8S 4L8, Canada;* orcid.org/0000-0002-2947-8580

**Stephen Yarwood** − *Institute of Biological Chemistry, Biophysics and Bioengineering, School of Engineering and Physical Sciences, Heriot-Watt University, Edinburgh EH14 4AS, United Kingdom*

Complete contact information is available at: https://pubs.acs.org/10.1021/acs.jmedchem.9b02151


### Author Contributions

The manuscript was written by H.S. and G.M. through the contributions of all authors. All authors have given approval to the final version of the manuscript.

### Notes

The authors declare no competing financial interest.

## ■ ACKNOWLEDGMENTS

We would like to express our appreciation to Dr. X. Cheng (UTHealth), Dr. M. Akimoto, R. Ahmed, and J. Huang for their helpful discussions. We thank Dr. K. Green, Dr. H. Jenkins, and Dr. B. Berno for technical assistance. This work was supported by Canadian Institutes of Health Research Grant 389522 (to G.M.) and Natural Sciences and Engineering Research Council of Canada Grant RGPIN-2019-05990 (to G.M.).

## ■ ABBREVIATIONS USED

BBR, base binding region; cAMP, cyclic adenosine monophosphate; CCS, compounded chemical shift; CHESCA, chemical shift covariance analysis; CHESPA, chemical shift projection analysis; CNBD, cyclic nucleotide-binding domain; EPAC, exchange protein directly activated by cAMP; GEF, guanine nucleotide exchange factor; GDP, guanosine diphosphate; GTP, guanosine triphosphate; HSQC, heteronuclear single quantum coherence; NMR, nuclear magnetic resonance; NOE, nuclear overhauser effect; PBC, phosphate binding



https://dx.doi.org/10.1021/acs.jmedchem.9b02151
J. Med. Chem. XXXX, XXX, XXX−XXX

cassette; STD, saturation transfer difference; STR, saturation transfer reference; WT, wild-type

## REFERENCES


(1) Kawasaki, H.; Springett, G. M.; Mochizuki, N.; Toki, S.; Nakaya, M.; Matsuda, M.; Housman, D. E.; Graybiel, A. M. A family of cAMP-binding proteins that directly activate Rap1. *Science* **1998**, *282*, 2275−2279.

(2) de Rooij, J.; Zwartkruis, F. J.; Verheijen, M. H.; Cool, R. H.; Nijman, S. M.; Wittinghofer, A.; Bos, J. L. Epac is a Rap1 guanine-nucleotide-exchange factor directly activated by cyclic AMP. *Nature* **1998**, *396*, 474−477.

(3) de Rooij, J.; Rehmann, H.; van Triest, M.; Cool, R. H.; Wittinghofer, A.; Bos, J. L. Mechanism of regulation of the Epac family of cAMP-dependent RapGEFs. *J. Biol. Chem.* **2000**, *275*, 20829−20836.

(4) Schmidt, M.; Dekker, F. J.; Maarsingh, H. Exchange protein directly activated by cAMP (epac): a multidomain cAMP mediator in the regulation of diverse biological functions. *Pharmacol. Rev.* **2013**, *65*, 670−709.

(5) Robichaux, W. G.; Cheng, X. Intracellular cAMP sensor EPAC: physiology, pathophysiology, and therapeutics development. *Physiol. Rev.* **2018**, *98*, 919−1053.

(6) Kaneko, M.; Takahashi, T. Presynaptic mechanism underlying cAMP-dependent synaptic potentiation. *J. Neurosci.* **2004**, *24*, 5202−5208.

(7) Yang, Y.; Shu, X.; Liu, D.; Shang, Y.; Wu, Y.; Pei, L.; Xu, X.; Tian, Q.; Zhang, J.; Qian, K.; Wang, Y.-X.; Petralia, R. S.; Tu, W.; Zhu, L.-Q.; Wang, J.-Z.; Lu, Y. EPAC null mutation impairs learning and social interactions via aberrant regulation of miR-124 and Zif268 translation. *Neuron* **2012**, *73*, 774−788.

(8) Morel, E.; Marcantoni, A.; Gastineau, M.; Birkedal, R.; Rochais, F.; Garnier, A.; Lompré, A.-M.; Vandecasteele, G.; Lezoualc'h, F. cAMP-binding protein Epac induces cardiomyocyte hypertrophy. *Circ. Res.* **2005**, *97*, 1296−1304.

(9) Métrich, M.; Lucas, A.; Gastineau, M.; Samuel, J.-L.; Heymes, C.; Morel, E.; Lezoualc'h, F. Epac mediates beta-adrenergic receptor-induced cardiomyocyte hypertrophy. *Circ. Res.* **2008**, *102*, 959−965.

(10) Laurent, A.-C.; Bisserier, M.; Lucas, A.; Tortosa, F.; Roumieux, M.; Régibus, A. de.; Swiader, A.; Sainte-Marie, Y.; Heymes, C.; Vindis, C.; Lezoualc'h, F. Exchange protein directly activated by cAMP 1 promotes autophagy during cardiomyocyte hypertrophy. *Cardiovasc. Res.* **2015**, *105*, 55−64.

(11) Fazal, L.; Laudette, M.; Paula-Gomes, S.; Pons, S.; Conte, C.; Tortosa, F.; Sicard, P.; Sainte-Marie, Y.; Bisserier, M.; Lairez, O.; Lucas, A.; Roy, J.; Ghaleb, B.; Fauconnier, J.; Mialet-Perez, J.; Lezoualc'h, F. Multifunctional mitochondrial Epac1 controls myocardial cell death. *Circ. Res.* **2017**, *120*, 645−657.

(12) Rangarajan, S.; Enserink, J. M.; Kuiperij, H. B.; de Rooij, J.; Price, L. S.; Schwede, F.; Bos, J. L. Cyclic AMP induces integrin-mediated cell adhesion through Epac and Rap1 upon stimulation of the beta 2-adrenergic receptor. *J. Cell Biol.* **2003**, *160*, 487−493.

(13) Bastian, P.; Balcarek, A.; Altanis, C.; Strell, C.; Niggemann, B.; Zaenker, K. S.; Entschladen, F. The inhibitory effect of norepinephrine on the migration of ES-2 ovarian carcinoma cells involves a Rap1-dependent pathway. *Cancer Lett.* **2009**, *274*, 218−224.

(14) Yan, J.; Mei, F. C.; Cheng, H.; Lao, D. H.; Hu, Y.; Wei, J.; Patrikeev, I.; Hao, D.; Stutz, S. J.; Dineley, K. T.; Motamedi, M.; Hommel, J. D.; Cunningham, K. A.; Chen, J.; Cheng, X. Enhanced leptin sensitivity, reduced adiposity, and improved glucose homeostasis in mice lacking exchange protein directly activated by cyclic AMP isoform 1. *Mol. Cell. Biol.* **2013**, *33*, 918−926.

(15) Almahariq, M.; Chao, C.; Mei, F. C.; Hellmich, M. R.; Patrikeev, I.; Motamedi, M.; Cheng, X. Pharmacological inhibition and genetic knockdown of exchange protein directly activated by cAMP 1 reduce pancreatic cancer metastasis in vivo. *Mol. Pharmacol.* **2015**, *87*, 142−149.

(16) Hu, Y.; Robichaux, W. G.; Mei, F. C.; Kim, E. R.; Wang, H.; Tong, Q.; Jin, J.; Xu, M.; Chen, J.; Cheng, X. Role of exchange protein directly activated by cyclic AMP isoform 1 in energy homeostasis: regulation of leptin expression and secretion in white adipose tissue. *Mol. Cell. Biol.* **2016**, *36*, 2440−2450.

(17) Gao, M.; Ma, Y.; Bast, R. C.; Li, Y.; Wan, L.; Liu, Y.; Sun, Y.; Fang, Z.; Zhang, L.; Wang, X.; Wei, Z. Epac1 knockdown inhibits the proliferation of ovarian cancer cells by inactivating AKT/Cyclin D1/CDK4 pathway in vitro and in vivo. *Med. Oncol.* **2016**, *33*, No. 73.

(18) Kumar, N.; Gupta, S.; Dabral, S.; Singh, S.; Sehrawat, S. Role of exchange protein directly activated by cAMP (EPAC1) in breast cancer cell migration and apoptosis. *Mol. Cell. Biochem.* **2017**, *430*, 115−125.

(19) Hwang, M.; Go, Y.; Park, J.-H.; Shin, S.-K.; Song, S. E.; Oh, B.-C.; Im, S.-S.; Hwang, I.; Jeon, Y. H.; Lee, I.-K.; Seino, S.; Song, D.-K. Epac2a-null mice exhibit obesity-prone nature more susceptible to leptin resistance. *Int. J. Obes.* **2017**, *41*, 279−288.

(20) Almahariq, M.; Tsalkova, T.; Mei, F. C.; Chen, H.; Zhou, J.; Sastry, S. K.; Schwede, F.; Cheng, X. A novel EPAC-specific inhibitor suppresses pancreatic cancer cell migration and invasion. *Mol. Pharmacol.* **2013**, *83*, 122−128.

(21) Wang, X.; Luo, C.; Cheng, X.; Lu, M. Lithium and an EPAC-specific inhibitor ESI-09 synergistically suppress pancreatic cancer cell proliferation and survival. *Acta Biochim. Biophys. Sin.* **2017**, *49*, 573−580.

(22) Gong, B.; Shelite, T.; Mei, F. C.; Ha, T.; Hu, Y.; Xu, G.; Chang, Q.; Wakamiya, M.; Ksiazek, T. G.; Boor, P. J.; Bouyer, D. H.; Popov, V. L.; Chen, J.; Walker, D. H.; Cheng, X. Exchange protein directly activated by cAMP plays a critical role in bacterial invasion during fatal rickettsioses. *Proc. Natl. Acad. Sci. U.S.A.* **2013**, *110*, 19615−19620.

(23) Tao, X.; Mei, F.; Agrawal, A.; Peters, C. J.; Ksiazek, T. G.; Cheng, X.; Tseng, C.-T. K. Blocking of exchange proteins directly activated by cAMP leads to reduced replication of Middle East respiratory syndrome coronavirus. *J. Virol.* **2014**, *88*, 3902−3910.

(24) Dawn, A.; Singh, S.; More, K. R.; Siddiqui, F. A.; Pachikara, N.; Ramdani, G.; Langsley, G.; Chitnis, C. E. The central role of cAMP in regulating Plasmodium falciparum merozoite invasion of human erythrocytes. *PLoS Pathog.* **2014**, *10*, No. e1004520.

(25) McPhee, I.; Gibson, L. C. D.; Kewney, J.; Darroch, C.; Stevens, P. A.; Spinks, D.; Cooreman, A.; MacKenzie, S. J. Cyclic nucleotide signalling: a molecular approach to drug discovery for Alzheimer's disease. *Biochem. Soc. Trans.* **2005**, *33*, 1330−1332.

(26) Singhmar, P.; Huo, X.; Eijkelkamp, N.; Berciano, S. R.; Baameur, F.; Mei, F. C.; Zhu, Y.; Cheng, X.; Hawke, D.; Mayor, F.; Murga, C.; Heijnen, C. J.; Kavelaars, A. Critical role for Epac1 in inflammatory pain controlled by GRK2-mediated phosphorylation of Epac1. *Proc. Natl. Acad. Sci. U.S.A.* **2016**, *113*, 3036−3041.

(27) Wang, H.; Heijnen, C. J.; van Velthoven, C. T. J.; Willemen, H. L. D. M.; Ishikawa, Y.; Zhang, X.; Sood, A. K.; Vroon, A.; Eijkelkamp, N.; Kavelaars, A. Balancing GRK2 and EPAC1 levels prevents and relieves chronic pain. *J. Clin. Invest.* **2013**, *123*, 5023−5034.

(28) Wan, X.; Torregrossa, M. M.; Sanchez, H.; Nairn, A. C.; Taylor, J. R. Activation of exchange protein activated by cAMP in the rat basolateral amygdala impairs reconsolidation of a memory associated with self-administered cocaine. *PLoS ONE* **2014**, *9*, No. e107359.

(29) Bos, J. L. Epac proteins: multi-purpose cAMP targets. *Trends Biochem. Sci.* **2006**, *31*, 680−686.

(30) Rehmann, H.; Das, J.; Knipscheer, P.; Wittinghofer, A.; Bos, J. L. Structure of the cyclic-AMP-responsive exchange factor Epac2 in its auto-inhibited state. *Nature* **2006**, *439*, 625−628.

(31) Mazhab-Jafari, M. T.; Das, R.; Fotheringham, S. A.; SilDas, S.; Chowdhury, S.; Melacini, G. Understanding cAMP-dependent allostery by NMR spectroscopy: comparative analysis of the EPAC1 cAMP-binding domain in its apo and cAMP-bound states. *J. Am. Chem. Soc.* **2007**, *129*, 14482−14492.

(32) VanSchouwen, B.; Selvaratnam, R.; Fogolari, F.; Melacini, G. Role of dynamics in the autoinhibition and activation of the exchange protein directly activated by cyclic AMP (EPAC). *J. Biol. Chem.* **2011**, *286*, 42655−42669.

(33) Das, R.; Mazhab-Jafari, M. T.; Chowdhury, S.; SilDas, S.; Selvaratnam, R.; Melacini, G. Entropy-driven cAMP-dependent allosteric control of inhibitory interactions in exchange proteins directly activated by cAMP. *J. Biol. Chem.* **2008**, *283*, 19691−19703.




https://dx.doi.org/10.1021/acs.jmedchem.9b02151
J. Med. Chem. XXXX, XXX, XXX−XXX

(34) Rehmann, H.; Arias-Palomo, E.; Hadders, M. A.; Schwede, F.; Llorca, O.; Bos, J. L. Structure of Epac2 in complex with a cyclic AMP analogue and RAP1B. *Nature* **2008**, *455*, 124−127.
(35) Rehmann, H.; Prakash, B.; Wolf, E.; Rueppel, A.; de Rooij, J.; Bos, J. L.; Wittinghofer, A. Structure and regulation of the cAMP-binding domains of Epac2. *Nat. Struct. Biol.* **2003**, *10*, 26−32.
(36) Kraemer, A.; Rehmann, H. R.; Cool, R. H.; Theiss, C.; de Rooij, J.; Bos, J. L.; Wittinghofer, A. Dynamic interaction of cAMP with the Rap guanine-nucleotide exchange factor Epac1. *J. Mol. Biol.* **2001**, *306*, 1167−1177.
(37) Kukic, P.; Alvin Leung, H. T.; Bemporad, F.; Aprile, F. A.; Kumita, J. R.; Simone, A. de.; Camilloni, C.; Vendruscolo, M. Structure and dynamics of the integrin LFA-1 I-domain in the inactive state underlie its inside-out/outside-in signaling and allosteric mechanisms. *Structure* **2015**, *23*, 745−753.
(38) Gagné, D.; Narayanan, C.; Doucet, N. Network of long-range concerted chemical shift displacements upon ligand binding to human angiogenin. *Protein Sci.* **2015**, *24*, 525−533.
(39) Cembran, A.; Kim, J.; Gao, J.; Veglia, G. NMR mapping of protein conformational landscapes using coordinated behavior of chemical shifts upon ligand binding. *Phys. Chem. Chem. Phys.* **2014**, *16*, 6508−6518.
(40) De, S.; Greenwood, A. I.; Rogals, M. J.; Kovrigin, E. L.; Lu, K. P.; Nicholson, L. K. Complete thermodynamic and kinetic characterization of the isomer-specific interaction between Pin1-WW domain and the amyloid precursor protein cytoplasmic tail phosphorylated at Thr668. *Biochemistry* **2012**, *51*, 8583−8596.
(41) Boehr, D. D.; Nussinov, R.; Wright, P. E. The role of dynamic conformational ensembles in biomolecular recognition. *Nat. Chem. Biol.* **2009**, *5*, 789−796.
(42) de Simone, A.; Aprile, F. A.; Dhulesia, A.; Dobson, C. M.; Vendruscolo, M. Structure of a low-population intermediate state in the release of an enzyme product. *eLife* **2015**, *4*, No. e02777.
(43) Selvaratnam, R.; VanSchouwen, B.; Fogolari, F.; Mazhab-Jafari, M. T.; Das, R.; Melacini, G. The projection analysis of NMR chemical shifts reveals extended EPAC autoinhibition determinants. *Biophys. J.* **2012**, *102*, 630−639.
(44) Tsalkova, T.; Mei, F. C.; Li, S.; Chepurny, O. G.; Leech, C. A.; Liu, T.; Holz, G. G.; Woods, V. L.; Cheng, X. Isoform-specific antagonists of exchange proteins directly activated by cAMP. *Proc. Natl. Acad. Sci. U.S.A.* **2012**, *109*, 18613−18618.
(45) Zhu, Y.; Chen, H.; Boulton, S.; Mei, F.; Ye, N.; Melacini, G.; Zhou, J.; Cheng, X. Biochemical and pharmacological characterizations of ESI-09 based EPAC inhibitors: defining the ESI-09 "therapeutic window". *Sci. Rep.* **2015**, *5*, No. 9344.
(46) Brown, L. M.; Rogers, K. E.; McCammon, J. A.; Insel, P. A. Identification and validation of modulators of exchange protein activated by cAMP (Epac) activity: structure-function implications for Epac activation and inhibition. *J. Biol. Chem.* **2014**, *289*, 8217−8230.
(47) Brown, L. M.; Rogers, K. E.; Aroonsakool, N.; McCammon, J. A.; Insel, P. A. Allosteric inhibition of Epac: computational modeling and experimental validation to identify allosteric sites and inhibitors. *J. Biol. Chem.* **2014**, *289*, 29148−29157.
(48) Laudette, M.; Coluccia, A.; Sainte-Marie, Y.; Solari, A.; Fazal, L.; Sicard, P.; Silvestri, R.; Mialet-Perez, J.; Pons, S.; Ghaleb, B.; Blondeau, J.-P.; Lezoualc'h, F. Identification of a pharmacological inhibitor of Epac1 that protects the heart against acute and chronic models of cardiac stress. *Cardiovasc. Res.* **2019**, *115*, 1766−1777.
(49) Courilleau, D.; Bisserier, M.; Jullian, J.-C.; Lucas, A.; Bouyssou, P.; Fischmeister, R.; Blondeau, J.-P.; Lezoualc'h, F. Identification of a tetrahydroquinoline analog as a pharmacological inhibitor of the cAMP-binding protein Epac. *J. Biol. Chem.* **2012**, *287*, 44192−44202.
(50) Courilleau, D.; Bouyssou, P.; Fischmeister, R.; Lezoualc'h, F.; Blondeau, J.-P. The R-enantiomer of CE3F4 is a preferential inhibitor of human exchange protein directly activated by cyclic AMP isoform 1 (Epac1). *Biochem. Biophys. Res. Commun.* **2013**, *440*, 443−448.
(51) Sonawane, Y. A.; Zhu, Y.; Garrison, J. C.; Ezell, E. L.; Zahid, M.; Cheng, X.; Natarajan, A. Structure-activity relationship studies with tetrahydroquinoline analogs as EPAC inhibitors. *ACS Med. Chem. Lett.* **2017**, *8*, 1183−1187.
(52) Boulton, S.; Selvaratnam, R.; Blondeau, J.-P.; Lezoualc'h, F.; Melacini, G. Mechanism of selective enzyme inhibition through uncompetitive regulation of an allosteric agonist. *J. Am. Chem. Soc.* **2018**, *140*, 9624−9637.
(53) Ahmed, A.; Boulton, S.; Shao, H.; Akimoto, M.; Natarajan, A.; Cheng, X.; Melacini, G. Recent advances in EPAC-targeted therapies: a biophysical perspective. *Cells* **2019**, *8*, 1462.
(54) Parnell, E.; McElroy, S. P.; Wiejak, J.; Baillie, G. L.; Porter, A.; Adams, D. R.; Rehmann, H.; Smith, B. O.; Yarwood, S. J. Identification of a novel, small molecule partial agonist for the cyclic AMP sensor, EPAC1. *Sci. Rep.* **2017**, *7*, No. 294.
(55) Schwede, F.; Maronde, E.; Genieser, H.-G.; Jastorff, B. Cyclic nucleotide analogs as biochemical tools and prospective drugs. *Pharmacol. Ther.* **2000**, *87*, 199−226.
(56) Enserink, J. M.; Christensen, A. E.; de Rooij, J.; van Triest, M.; Schwede, F.; Genieser, H. G.; Døskeland, S. O.; Blank, J. L.; Bos, J. L. A novel Epac-specific cAMP analogue demonstrates independent regulation of Rap1 and ERK. *Nat. Cell Biol.* **2002**, *4*, 901−906.
(57) Christensen, A. E.; Selheim, F.; de Rooij, J.; Dremier, S.; Schwede, F.; Dao, K. K.; Martinez, A.; Maenhaut, C.; Bos, J. L.; Genieser, H.-G.; Døskeland, S. O. cAMP analog mapping of Epac1 and cAMP kinase. Discriminating analogs demonstrate that Epac and cAMP kinase act synergistically to promote PC-12 cell neurite extension. *J. Biol. Chem.* **2003**, *278*, 35394−35402.
(58) Rehmann, H.; Schwede, F.; Døskeland, S. O.; Wittinghofer, A.; Bos, J. L. Ligand-mediated activation of the cAMP-responsive guanine nucleotide exchange factor Epac. *J. Biol. Chem.* **2003**, *278*, 38548−38556.
(59) Poppe, H.; Rybalkin, S. D.; Rehmann, H.; Hinds, T. R.; Tang, X.-B.; Christensen, A. E.; Schwede, F.; Genieser, H.-G.; Bos, J. L.; Doskeland, S. O.; Beavo, J. A.; Butt, E. Cyclic nucleotide analogs as probes of signaling pathways. *Nat. Methods* **2008**, *5*, 277−278.
(60) Vliem, M. J.; Ponsioen, B.; Schwede, F.; Pannekoek, W.-J.; Riedl, J.; Kooistra, M. R. H.; Jalink, K.; Genieser, H.-G.; Bos, J. L.; Rehmann, H. 8-pCPT-2′-O-Me-cAMP-AM: an improved Epac-selective cAMP analogue. *ChemBioChem* **2008**, *9*, 2052−2054.
(61) Dodge-Kafka, K. L.; Soughayer, J.; Pare, G. C.; Carlisle Michel, J. J.; Langeberg, L. K.; Kapiloff, M. S.; Scott, J. D. The protein kinase A anchoring protein mAKAP coordinates two integrated cAMP effector pathways. *Nature* **2005**, *437*, 574−578.
(62) Conti, M.; Beavo, J. Biochemistry and physiology of cyclic nucleotide phosphodiesterases: essential components in cyclic nucleotide signaling. *Annu. Rev. Biochem.* **2007**, *76*, 481−511.
(63) Wiejak, J.; van Basten, B.; Luchowska-Stańska, U.; Hamilton, G.; Yarwood, S. J. The novel exchange protein activated by cyclic AMP 1 (EPAC1) agonist, I942, regulates inflammatory gene expression in human umbilical vascular endothelial cells (HUVECs). *Biochim. Biophys. Acta Mol. Cell Res.* **2019**, *1866*, 264−276.
(64) Barker, G.; Parnell, E.; van Basten, B.; Buist, H.; Adams, D. R.; Yarwood, S. J. The potential of a novel class of EPAC-selective agonists to combat cardiovascular Inflammation. *J. Cardiovasc. Dev. Dis.* **2017**, *4*, 22.
(65) Tsalkova, T.; Mei, F. C.; Cheng, X. A fluorescence-based high-throughput assay for the discovery of exchange protein directly activated by cyclic AMP (EPAC) antagonists. *PLoS ONE* **2012**, *7*, No. e30441.
(66) Boulton, S.; Selvaratnam, R.; Ahmed, R.; Van, K.; Cheng, X.; Melacini, G. Mechanisms of specific versus nonspecific interactions of aggregation-prone inhibitors and attenuators. *J. Med. Chem.* **2019**, *62*, 5063−5079.
(67) Selvaratnam, R.; Chowdhury, S.; VanSchouwen, B.; Melacini, G. Mapping allostery through the covariance analysis of NMR chemical shifts. *Proc. Natl. Acad. Sci. U.S.A.* **2011**, *108*, 6133−6138.
(68) Eghbalnia, H. R.; Wang, L.; Bahrami, A.; Assadi, A.; Markley, J. L. Protein energetic conformational analysis from NMR chemical shifts (PECAN) and its use in determining secondary structural elements. *J. Biomol. NMR* **2005**, *32*, 71−81.


https://dx.doi.org/10.1021/acs.jmedchem.9b02151
J. Med. Chem. XXXX, XXX, XXX−XXX

(69) Zwahlen, C.; Legault, P.; Vincent, S. J. F.; Greenblatt, J.; Konrat, R.; Kay, L. E. Methods for measurement of intermolecular NOEs by multinuclear NMR spectroscopy: application to a bacteriophage λ N-peptide/ boxB RNA complex. *J. Am. Chem. Soc.* **1997**, *119*, 6711−6721.
(70) Melacini, G. Separation of intra- and intermolecular NOEs through simultaneous editing and J -compensated filtering: A 4D quadrature-free constant-time J -resolved approach. *J. Am. Chem. Soc.* **2000**, *122*, 9735−9738.
(71) Medek, A.; Hajduk, P. J.; Mack, J.; Fesik, S. W. The use of differential chemical shifts for determining the binding site location and orientation of protein-bound ligands. *J. Am. Chem. Soc.* **2000**, *122*, 1241−1242.
(72) Mayer, M.; Meyer, B. Group epitope mapping by saturation transfer difference NMR to identify segments of a ligand in direct contact with a protein receptor. *J. Am. Chem. Soc.* **2001**, *123*, 6108−6117.
(73) Das, R.; Chowdhury, S.; Mazhab-Jafari, M. T.; SilDas, S.; Selvaratnam, R.; Melacini, G. Dynamically driven ligand selectivity in cyclic nucleotide binding domains. *J. Biol. Chem.* **2009**, *284*, 23682−23696.
(74) Delaglio, F.; Grzesiek, S.; Vuister, G. W.; Zhu, G.; Pfeifer, J.; Bax, A. NMRPipe: a multidimensional spectral processing system based on UNIX pipes. *J. Biomol. NMR* **1995**, *6*, 277−293.
(75) Goddard, T. D.; Kneller, D. G.*Sparky 3*; University of California: San Francisco, 2008.
(76) Yamazaki, T.; Pascal, S. M.; Singer, A. U.; Forman-Kay, J. D.; Kay, L. E. NMR pulse schemes for the sequence-specific assignment of arginine guanidino 15N and 1H chemical shifts in proteins. *J. Am. Chem. Soc.* **1995**, *117*, 3556−3564.
(77) Wang, Z.-X. An exact mathematical expression for describing competitive binding of two different ligands to a protein molecule. *FEBS Lett.* **1995**, *360*, 111−114.
(78) Byun, J. A.; Melacini, G. NMR methods to dissect the molecular mechanisms of disease-related mutations (DRMs): Understanding how DRMs remodel functional free energy landscapes. *Methods* **2018**, *148*, 19−27.
(79) de Hoon, M. J. L.; Imoto, S.; Nolan, J.; Miyano, S. Open source clustering software. *Bioinformatics* **2004**, *20*, 1453−1454.
(80) Wang, P.; Luchowska-Stańska, U.; Chen, H.; Liu, Z.; Wiejak, J.; Whelan, P.; Morgan, D.; Lochhead, E.; Barker, G.; Rehmann, H.; Yarwood, S. J.; Zhou, J. Synthesis and biochemical evaluation of non-cyclic nucleotide exchange protein directly activated by cAMP (EPAC) partial agonists. Unpublished results.
(81) VanSchouwen, B.; Selvaratnam, R.; Giri, R.; Lorenz, R.; Herberg, F. W.; Kim, C.; Melacini, G. Mechanism of cAMP partial agonism in protein kinase G (PKG). *J. Biol. Chem.* **2015**, *290*, 28631−28641.
(82) Boulton, S.; Melacini, G. Advances in NMR methods to map allosteric sites: from models to translation. *Chem. Rev.* **2016**, *116*, 6267−6304.


https://dx.doi.org/10.1021/acs.jmedchem.9b02151
*J. Med. Chem.* XXXX, XXX, XXX−XXX